

# THE DEEP3 GALAXY REDSHIFT SURVEY: THE IMPACT OF ENVIRONMENT ON THE SIZE EVOLUTION OF MASSIVE EARLY-TYPE GALAXIES AT INTERMEDIATE REDSHIFT<sup>†‡</sup>

MICHAEL C. COOPER<sup>1,∇</sup>, ROGER L. GRIFFITH<sup>2</sup>, JEFFREY A. NEWMAN<sup>3</sup>, ALISON L. COIL<sup>4,‡</sup>, MARC DAVIS<sup>5,6</sup>, AARON A. DUTTON<sup>7,b</sup>, S. M. FABER<sup>8</sup>, PURAGRA GUHATHAKURTA<sup>8</sup>, DAVID C. KOO<sup>8</sup>, JENNIFER M. LOTZ<sup>9</sup>, BENJAMIN J. WEINER<sup>10</sup>, CHRISTOPHER N. A. WILLMER<sup>10</sup>, RENBIN YAN<sup>11</sup>

*Draft version August 8, 2018*

## ABSTRACT

Using data drawn from the DEEP2 and DEEP3 Galaxy Redshift Surveys, we investigate the relationship between the environment and the structure of galaxies residing on the red sequence at intermediate redshift. Within the massive ( $10 < \log_{10}(M_*/h^{-2} M_\odot) < 11$ ) early-type population at  $0.4 < z < 1.2$ , we find a significant correlation between local galaxy overdensity (or environment) and galaxy size, such that early-type systems in higher-density regions tend to have larger effective radii (by  $\sim 0.5 h^{-1}$  kpc or 25% larger) than their counterparts of equal stellar mass and Sérsic index in lower-density environments. This observed size-density relation is consistent with a model of galaxy formation in which the evolution of early-type systems at  $z < 2$  is accelerated in high-density environments such as groups and clusters and in which dry, minor mergers (versus mechanisms such as quasar feedback) play a central role in the structural evolution of the massive, early-type galaxy population.

*Subject headings:* galaxies:statistics, galaxies:fundamental parameters, galaxies:high-redshift, galaxies:formation, galaxies:evolution, large-scale structure of universe

## 1. INTRODUCTION

Recent observations of galaxies at intermediate redshift ( $z \sim 2$ ) have identified a significant popu-

<sup>†</sup> Some of the data presented herein were obtained at the W.M. Keck Observatory, which is operated as a scientific partnership among the California Institute of Technology, the University of California and the National Aeronautics and Space Administration. The Observatory was made possible by the generous financial support of the W.M. Keck Foundation.

<sup>‡</sup> Based on observations made with the NASA/ESA Hubble Space Telescope, obtained from the data archive at the Space Telescope Science Institute. STScI is operated by the Association of Universities for Research in Astronomy, Inc. under NASA contract NAS 5-26555.

<sup>1</sup> Center for Galaxy Evolution, Department of Physics and Astronomy, University of California, Irvine, 4129 Frederick Reines Hall, Irvine, CA 92697, USA; m.cooper@uci.edu

<sup>∇</sup> Hubble Fellow

<sup>2</sup> Infrared Processing and Analysis Center, California Institute of Technology, Pasadena, CA 91125, USA

<sup>3</sup> Department of Physics and Astronomy, University of Pittsburgh, 3941 O'Hara Street, Pittsburgh, PA 15260, USA

<sup>4</sup> Department of Physics, Center for Astrophysics and Space Sciences, University of California, San Diego, 9500 Gilman Drive, La Jolla, CA, 92093

<sup>‡</sup> Alfred P. Sloan Foundation Fellow

<sup>5</sup> Department of Astronomy, University of California, Berkeley, Hearst Field Annex B, Berkeley, CA 94720, USA

<sup>6</sup> Department of Physics, University of California, Berkeley, 366 LeConte Hall MC 7300, Berkeley, CA 94720, USA

<sup>7</sup> Department of Physics and Astronomy, University of Victoria, Victoria B.C., V8P 5C2, Canada

<sup>b</sup> CITA National Fellow

<sup>8</sup> UCO/Lick Observatory and Department of Astronomy and Astrophysics, University of California, Santa Cruz, 1156 High Street, Santa Cruz, CA 95064, USA

<sup>9</sup> Space Telescope Science Institute, 3700 San Martin Drive, Baltimore, MD 21218, USA

<sup>10</sup> Steward Observatory, University of Arizona, 933 N. Cherry Avenue, Tucson, AZ 85721, USA

<sup>11</sup> Center for Cosmology and Particle Physics, Department of Physics, New York University, 4 Washington Place, New York, NY 10003, USA

lation of massive ( $\sim 10^{11} M_\odot$ ), quiescent, early-type systems with old, metal-rich stellar populations and remarkably small sizes relative to their local counterparts (e.g., Daddi et al. 2005; Labbé et al. 2005; Papovich et al. 2006; Kriek et al. 2006; Trujillo et al. 2006, 2007; Zirm et al. 2007; van Dokkum et al. 2008; Damjanov et al. 2009, 2011; Toft et al. 2009; Taylor et al. 2010). The stellar densities of these massive, intermediate-redshift galaxies (as measured within one effective radius,  $r_e$ ) are typically two orders of magnitude greater than quiescent ellipticals of the same mass at  $z \sim 0.1$ . Within the central 1 kpc (physical), however, the densities of early-types at  $z \sim 2$  are found to only exceed local measurements by a factor of 2–3 (Bezanson et al. 2009; Hopkins et al. 2009a; van Dokkum et al. 2010). Altogether, the observations suggest that there is significant evolution in the size of massive ellipticals over the past 10 Gyr, likely proceeding in an inside-out manner, without the addition of much stellar mass.

Several physical processes have been proposed to explain this strong size evolution within the massive, early-type population at  $z < 2$ . In particular, gas-poor, collisionless (or “dry”) minor mergers are often invoked as a means for puffing up the stellar component of these massive systems (e.g., Naab et al. 2006, 2007, 2009; Khochfar & Silk 2006; Bournaud et al. 2007; Boylan-Kolchin & Ma 2007; van der Wel et al. 2009; Cenarro & Trujillo 2009; Hopkins et al. 2009b, 2010a; Trujillo et al. 2011). However, a variety of alternative mechanisms have also been proposed, including scenarios in which the observed structural evolution may be driven by secular processes such as adiabatic expansion resulting from stellar mass loss and/or strong AGN-fueled feedback (Fan et al. 2008, 2010; Damjanov et al. 2009; Hopkins et al. 2010b,a; see also Nipoti et al. 2009 and

Williams et al. 2010).

One way to possibly discriminate between these scenarios (minor mergers versus secular processes) is by quantifying the role of environment in the structural evolution of the massive galaxy population. While secular processes are largely independent of environment and quasars are not preferentially found in overdense regions at  $z \sim 1$  (Coil et al. 2007), mergers are more common in higher-density environments such as galaxy groups (Cavaliere et al. 1992; McIntosh et al. 2008; Wetzel et al. 2008; Fakhouri & Ma 2009; Lin et al. 2010; Darg et al. 2010). Thus, if mergers are the dominant mechanism by which the sizes of massive early-types evolve at  $z < 2$ , we should expect to find a variation in the structural properties of galaxies as a function of environment at  $z \sim 1$ .

To test this, we use data drawn from the DEEP2 and DEEP3 Galaxy Redshift Surveys (Davis et al. 2003; Newman et al. 2012; Cooper et al. 2011) to investigate the correlation between the local overdensity of galaxies (which we generally refer to as “environment”) and the sizes of massive galaxies on the red sequence at intermediate redshift. In Section 2, we describe our data set, with results and discussion presented in Sections 3 and 4, respectively. Throughout, we employ a  $\Lambda$ CDM cosmology with  $w = -1$ ,  $\Omega_m = 0.3$ ,  $\Omega_\Lambda = 0.7$ , and a Hubble parameter of  $H_0 = 100 h \text{ km s}^{-1} \text{ Mpc}^{-1}$ , unless otherwise noted. All magnitudes are on the AB system (Oke & Gunn 1983).

## 2. DATA

To characterize both the environment and the structure of galaxies accurately requires spectroscopic observations (or deep, multi-band photometric observations, Cooper et al. 2005) as well as high-resolution imaging across a sizable area of sky. Given the limitations of ground-based adaptive-optics observations, the latter is only possible at intermediate redshift via space-based observations (e.g., with *HST*). Among the fields covered by deep, multi-band imaging with *HST*, the Extended Groth Strip (EGS) is by far the most complete with regard to spectroscopic coverage at intermediate redshift. The EGS is one of four fields surveyed by the DEEP2 Galaxy Redshift Survey (Davis et al. 2003, 2007; Newman et al. 2012), yielding high-precision ( $\sigma_z \sim 30 \text{ km s}^{-1}$ ) secure redshifts for 11,701 sources at  $0.2 < z < 1.4$  over roughly 0.5 square degrees in the EGS. Building upon the DEEP2 spectroscopic sample, the recently-completed DEEP3 Galaxy Redshift Survey (Cooper et al. 2011; Cooper et al., in prep) has brought the target sampling rate to  $\sim 90\%$  at  $R_{\text{AB}} < 24.1$  over the central 0.25 square degrees of the EGS — the portion of the field imaged by *HST*/ACS (see Fig. 1; Davis et al. 2007; Lotz et al. 2008).

Among the current generation of deep spectroscopic redshift surveys at  $z \sim 1$ , the combination of the DEEP2 and DEEP3 spectroscopic datasets provides the largest sample of accurate spectroscopic redshifts, the highest-precision velocity information, and the highest sampling density (Newman et al. 2012; Cooper et al., in prep).<sup>17</sup>

<sup>17</sup> Note that the sampling density for a survey is defined to be the number of galaxies with an accurate redshift measurement per unit of comoving volume and *not* the number of galaxies targeted

Combined with the relatively wide area imaged with *HST*/ACS (an area  $> 2\times$  larger than that surveyed as part of the GOODS program, Giavalisco et al. 2004), these attributes make the EGS one of the best-suited fields in which to study the relationship between environment and galaxy structure at  $z \sim 1$ . In this paper, we utilize a parent sample of 11,493 galaxies drawn from the joint DEEP2/DEEP3 dataset in the EGS with secure redshifts (quality  $Q = 3$  or 4 as defined by Davis et al. 2007; Newman et al. 2012) in the range  $0.4 < z < 1.2$ .

### 2.1. Rest-frame Colors, Luminosities, and Stellar Masses

For each galaxy in the DEEP2/DEEP3 sample, rest-frame  $U - B$  colors and absolute  $B$ -band magnitudes,  $M_B$ , are calculated from CFHT *BRI* photometry (Coil et al. 2004) using the  $K$ -correction procedure described in Willmer et al. (2006). For a subset of the galaxy catalog, stellar masses are calculated by fitting spectral energy distributions (SEDs) to WIRC/Palomar  $J$ - and  $K_s$ -band photometry in conjunction with the DEEP2 *BRI* data, according to the prescriptions described by Bundy et al. (2005, 2006). However, the near-infrared photometry, collected as part of the Palomar Observatory Wide-field Infrared (POWIR, Conselice et al. 2008) survey, does not cover the entire DEEP2/DEEP3 survey area, and often faint blue galaxies at the high- $z$  end of the DEEP2 redshift range are not detected in  $K_s$ . Because of these two effects, the stellar masses of Bundy et al. (2006) have been used to calibrate stellar mass estimates for the full DEEP2 sample that are based on rest-frame  $M_B$  and  $B - V$  values derived from the DEEP2 data in conjunction with the expressions of Bell et al. (2003), which relate mass-to-light ratio to optical color. We empirically correct these stellar mass estimates to the Bundy et al. (2006) measurements by accounting for a mild color and redshift dependence (Lin et al. 2007); where they overlap, the two stellar masses have an rms difference of approximately 0.3 dex after this calibration.

### 2.2. Local Galaxy Overdensity

To characterize the local environment, we compute the projected third-nearest-neighbor surface density ( $\Sigma_3$ ) about each galaxy in the joint DEEP2/DEEP3 sample, where the surface density depends on the projected distance to the third-nearest neighbor,  $D_{p,3}$ , as  $\Sigma_3 = 3/(\pi D_{p,3}^2)$ . In computing  $\Sigma_3$ , a velocity window of  $\pm 1250 \text{ km s}^{-1}$  is utilized to exclude foreground and background galaxies along the line of sight. Varying the width of this velocity window (e.g., using  $\pm 1000$ – $2000 \text{ km s}^{-1}$ ) or tracing environment according to the projected distance to the fifth-nearest neighbor has no significant effect on our results. In the tests of Cooper et al. (2005), this projected  $n^{\text{th}}$ -nearest-neighbor environment estimator proved to be the most robust indicator of local galaxy density for the DEEP2 survey.

To correct for the redshift dependence of the DEEP2 and DEEP3 sampling rates, each surface density value is divided by the median  $\Sigma_3$  of galaxies at that redshift within a window of  $\Delta z = 0.04$ ; correcting the measured

down to an arbitrary magnitude limit.

surface densities in this manner converts the  $\Sigma_3$  values into measures of overdensity relative to the median density (given by the notation  $1 + \delta_3$  here) and effectively accounts for the redshift variations in the selection rate (Cooper et al. 2005). Finally, to minimize the effects of edges and holes in the survey geometry, we exclude all galaxies within  $1 h^{-1}$  comoving Mpc of the DEEP3 survey boundary (see Fig. 1), reducing our sample to 7,257 galaxies in the redshift range  $0.4 < z < 1.2$ .

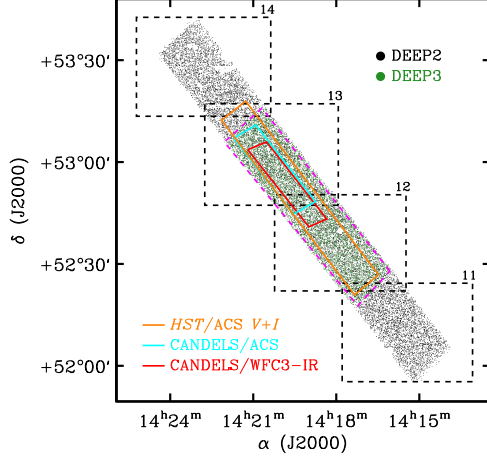


FIG. 1.— DEEP2 and DEEP3 spectroscopic coverage in the Extended Groth Strip. The black and green points denote the spectroscopic targets of the two surveys, with the area covered by *HST*/ACS imaging highlighted in orange. The dashed magenta line denotes the edge of the DEEP3 survey and thus the area over which environments were computed for this work. The areas to be imaged with *HST*/ACS and WFC3-IR as part of the CANDELS Multi-Cycle Treasury Program (Grogin et al. 2011) are delineated by the cyan and red outlines, respectively. Finally, the location of the four CFHT pointings (numbered 11–14) imaged by Coil et al. (2004) are denoted by the black dashed lines.

### 2.3. Sérsic Indices and Sizes

To quantify the sizes of the DEEP2 and DEEP3 galaxies, we utilize morphological measurements extracted from the Advanced Camera for Surveys General Catalog (ACS-GC, Griffith et al. 2012, in prep). The ACS-GC analyzed the *HST*/ACS  $V_{F606W}$  and  $I_{F814W}$  imaging in the EGS using GALAPAGOS (Häußler et al. 2011), a semi-automated tool for measuring sizes and spatial profiles via the parametric fitting code GALFIT (Peng et al. 2002, 2010). To determine the galaxy profile shape, each radial profile was fit using a simple Sérsic measurement (Sérsic 1968) of the form

$$\Sigma(r) = \Sigma_e \exp[-\kappa((r/r_e)^{-n} - 1)] \quad (1)$$

where  $r_e$  is the effective radius of the galaxy,  $\Sigma_e$  is the surface brightness at  $r_e$ ,  $n$  is the power-law index, and  $\kappa$  is coupled to  $n$  such that half of the total flux is always within  $r_e$ .

Here, we employ the profile fits to the *HST*/ACS  $I_{F814W}$  imaging for all sources, independent of galaxy redshift. At  $z < 1.2$ , the  $I_{F814W}$  passband samples the rest-frame optical ( $\lambda > 3700\text{\AA}$ ), which minimizes morphological biases associated with observations made in

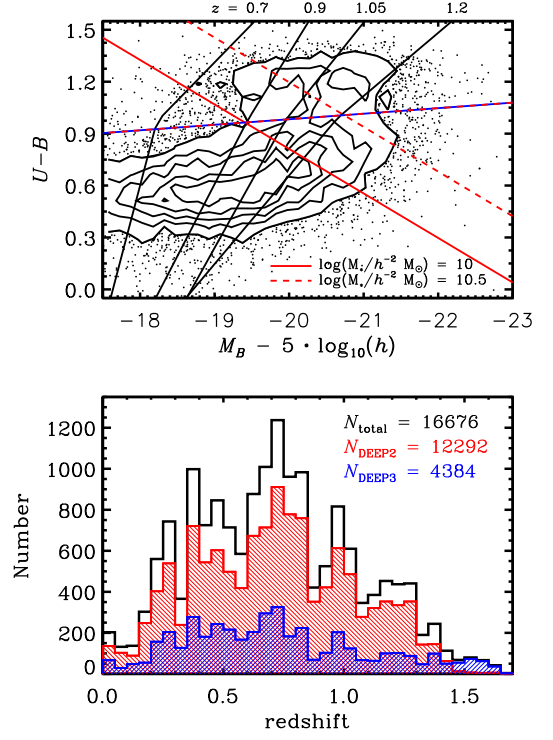


FIG. 2.— *Top*: the rest-frame  $U-B$  versus  $M_B$  color-magnitude distribution for the DEEP2 and DEEP3 galaxies in the spectroscopic sample within the redshift range  $0.4 < z < 1.2$ . The four solid black lines show the effective absolute-magnitude limit of the survey at  $z = 0.7, 0.9, 1.05, \text{ and } 1.2$ , while the solid and dashed red lines show lines of constant stellar mass corresponding to  $\log_{10}(M_*/h^{-2} M_\odot) = 10$  and  $10.5$ , respectively. The dashed blue/red horizontal line shows the division between the red sequence and the blue cloud as given by Equation 19 of Willmer et al. (2006). *Bottom*: the combined distribution of the 16,676 unique, secure ( $Q = -1, 3, 4$ ) redshifts measured by DEEP2 and DEEP3 within the Extended Groth Strip field (black histogram). The red and blue histograms show the corresponding distributions for the DEEP2 and DEEP3 surveys independently. Recall that the DEEP2 survey covers roughly a factor of 2 more area than the DEEP3 survey (see Fig. 1).

the rest-frame ultraviolet where galaxies typically exhibit more irregular morphologies. The impact (or lack thereof) of any morphological  $K$ -correction is addressed further in §3. Throughout our analysis, all sizes ( $r_e$ ) have been converted to physical kpc, according to the DEEP2/DEEP3 spectroscopic redshift and assuming a Hubble parameter of  $h = 1$ . Finally, note that the multidrizzled *HST*/ACS images, from which structural properties were measured, have a pixel scale of  $0.03''$  per pixel and a point-spread function (PSF) of  $0.12''$  FWHM; from  $z = 0.4$  to  $z = 1.2$ , the spatial resolution therefore varies from  $\sim 0.5 h^{-1}$  kpc per PSF FWHM to  $\sim 0.95 h^{-1}$  kpc per PSF FWHM.

### 2.4. Sample Selection

To investigate the relationship between galaxy structure and environment amongst the high-mass portion of the red sequence, we define a subsample of DEEP2/DEEP3 galaxies at  $0.4 < z < 1.2$  with stellar mass in the range  $10 < \log_{10}(M_*/h^{-2} M_\odot) < 11$ , on the



red sequence (i.e., rest-frame color of  $U - B > 1$ ),<sup>18</sup> and with robust environment and morphology measurements (i.e., away from a survey edge and with  $\sigma_n < 0.75$ ).<sup>19</sup> The median redshift for this subsample of 623 galaxies is 0.76 and the median stellar mass is  $\log_{10}(M_*/h^{-2} M_\odot) \sim 10.6$ .

In Figure 2, we show the redshift distribution for all sources in the EGS with a secure redshift ( $Q = -1, 3, 4$ ) in the joint DEEP2/DEEP3 sample alongside the color-magnitude distribution for all galaxies at  $0.4 < z < 1.2$ , with lines of constant stellar mass overlaid and with lines illustrating the survey magnitude limit at several discrete redshift values. Note that we restrict our primary subsample to a redshift range over which the DEEP2 and DEEP3 selection function is relatively flat. However, over this somewhat broad redshift range the sample is incomplete at the adopted mass limit. For example, at  $z = 0.9$  the  $R_{AB} = 24.1$  magnitude limit of DEEP2 includes all galaxies with stellar mass  $> 10^{10.8} M_*/h^{-2} M_\odot$  independent of color, but preferentially misses red galaxies at lower masses (see Fig. 2). This incompleteness in the galaxy population is addressed in more detail in §3.

### 3. ANALYSIS

In order to study the relationship between galaxy properties and environment at fixed stellar mass, as we aim to do here, the galaxy sample under study is often restricted to a narrow range in stellar mass such that correlations between stellar mass and environment are negligible. However, at intermediate redshift, sample sizes are generally limited in number such that using a particularly narrow stellar mass range (e.g.,  $\sim 0.1$ – $0.2$  dex in width) significantly reduces the statistical power of the sample. For this reason, broader stellar mass bins (e.g.,  $\sim 0.5$  dex) are commonly employed. However, if the shape of the stellar mass function depends on environment (as suggested by Balogh et al. 2001; Kauffmann et al. 2004; Croton et al. 2005; Baldry et al. 2006; Rudnick et al. 2009; Cooper et al. 2010b; Bolzonella et al. 2010), then the typical stellar mass within a broad mass bin may differ significantly from one density regime to another. Such an effect would clearly impact the ability to study the relationship between galaxy size and environment at fixed stellar mass.

For this reason, we instead select those galaxies within the top 15% of the overdensity distribution for all red galaxies at  $10 < \log_{10}(M_*/h^{-2} M_\odot) < 11$  and  $0.4 < z < 1.2$  (a subsample of 93 galaxies), and from the corresponding bottom 50% of the overdensity distribution we randomly draw 1000 subsamples (each composed of 93 galaxies) so as to match the joint redshift, stellar mass, and Sérsic index distributions of the galaxies in the high-density subsample.<sup>20</sup> The average environment for the high-density subset is  $\log_{10}(1 + \delta_3) = 1.31$ , with an in-

terquartile (25%–75%) range of 1.15–1.41, while the low-density subsample is biased to considerably less-dense environs with an average overdensity of  $\log_{10}(1 + \delta_3) = -0.12$  and an interquartile range of  $-0.30$ – $0.12$ . As shown by Cooper et al. (2006), the high-density subsample is comprised largely of group members, while the low-density population is dominated by “field” galaxies (see also Cooper et al. 2007; Gerke et al. 2007).

By matching in redshift, we remove the projection of any possible residual correlation between our environment measurements and redshift (in concert with the known redshift dependence of the survey’s stellar-mass limit) onto the observed size-environment relation. In addition, matching according to redshift alleviates any possible impact from morphological  $K$ -corrections associated with measuring all structural parameters in the *HST*/ACS  $I_{F814W}$  passband. Finally, recognizing the correlations between environment and parameters such as color, star-formation rate, and morphology (i.e., early- versus late-type) at  $z \sim 1$  (e.g., Cooper et al. 2006, 2008, 2010b; Capak et al. 2007; Elbaz et al. 2007; van der Wel et al. 2007), we also force the Sérsic indices of the low-density subsample to match those of the high-density population, which controls for the contribution of dusty disk galaxies to our red-sequence population. Matching based on rest-frame color, in lieu of Sérsic index, would confuse reddened disk galaxies with red early-type systems.

Members of the low-density subsample are drawn randomly from within a three-dimensional window with dimensions of  $|\Delta z| < 0.04$ ,  $|\Delta \log_{10}(M_*/h^{-2} M_\odot)| < 0.2$ , and  $|\Delta n| < 1.5$  of a randomly-selected object in the high-density subsample. Varying the size of this window by factors of a few in each dimension has no significant effect on our results. Given the random nature of the matching, some objects are repeated in the low-density subsamples. However, for each subsample of 93 galaxies,  $> 70\%$  of the galaxies are unique; requiring all members of a subsample to be unique would skew the statistics (Efron 1981). By matching our high- and low-density subsamples in stellar mass, redshift, as well as Sérsic index, we are able to effectively study the correlation between galaxy size and environment at fixed stellar mass.

To test whether our high-density subsample and the random low-density subsamples are consistent with being drawn from the same underlying stellar mass distribution, we apply two non-parametric (i.e., independent of Gaussian assumptions) tests, the two-sided Kolmogorov-Smirnov (KS) test (Press et al. 1986; Wall & Jenkins 2003) and the one-sided Wilcoxon-Mann-Whitney (WMW)  $U$  test (Mann & Whitney 1947). The result of each test is a  $P$ -value: the probability that a value of the KS or  $U$  statistic equal to the observed value or more extreme would be obtained, if the “null” hypothesis holds that the samples are drawn from the same parent distribution. The WMW  $U$  test is computed by ranking all elements of the two data sets together and then comparing the mean (or total) of the ranks from each data set. Because it relies on ranks rather than observed values, it is highly robust to non-Gaussianity. The WMW  $U$  test is particularly useful for small data sets (e.g., compared to other related tests such as the chi-square two-sample test, Wall & Jenkins 2003), as we have when selecting galaxies from a narrow stel-

<sup>18</sup> We adopt this simplified color-cut to be more restrictive at the faint end of the red sequence, where dusty star-forming galaxies are more prominent (Lotz et al. 2008). However, using a luminosity-dependent color-cut (e.g., Equation 19 of Willmer et al. 2006) yields no significant changes in our results.

<sup>19</sup> Limiting the sample to those sources with  $\sigma_n < 0.75$  excludes very few (only 2 out of 625) objects. Removing this selection criterion or making it more restrictive (e.g.,  $\sigma_n < 0.5$ ) yields no significant changes in our results.

<sup>20</sup> Selecting the top 10% or 20% of the environment distribution yields similar results.

lar mass range and in extreme environments, due to its insensitivity to outlying data points, its avoidance of binning, and its high efficiency. Note that since this test is one-sided, possible  $P_U$  values range from 0 to 0.5 (versus  $P_{KS}$  which ranges from 0 to 1); for a  $P_U$  value below 0.025 (corresponding closely to  $2\sigma$  for a Gaussian), we can reject the null hypothesis (that the two samples have the same distribution) at greater than 95% significance.<sup>21</sup>

In Figure 3, we plot the cumulative distribution of stellar masses for the 93 sources in the high-density subsample alongside that for the 1000 random subsamples (each consisting of 93 galaxies) matched in redshift but residing in low-density environments. Performing a one-sided WMW  $U$  test (and a two-sided KS test) on the size ( $r_e$ ) measurements for the low- and high-density populations, we find that the size distribution for the galaxies in high-density environments is skewed to larger sizes, with a probability of  $P_U < 0.01$  (and  $P_{KS} < 0.02$ ). Meanwhile, the cumulative stellar mass, redshift, and Sérsic index distributions for the low- and high-density subsamples, shown in the inset of Figure 3, are well-matched with the WMW  $U$  test yielding a  $P_U > 0.4$ . This confirms that our sample-construction procedure has yielded sets of galaxies in low- and high-density environments whose redshift, mass, and Sérsic index distributions match closely. While not directly matched, the rest-frame color distributions for the two samples are also indistinguishable — not a surprising result given that the color-density relation shows no significant variation across the red sequence at a given luminosity (Blanton et al. 2005; Cooper et al. 2006). See Table 1 for a complete summary of the probability values given by both the WMW  $U$  and KS tests.

The results of the WMW  $U$  test are confirmed by a comparison of the Hodges-Lehmann (H-L) estimator of the mean sizes for the low- and high-density subsamples, which differ by  $0.54 \pm 0.22 h^{-1}$  kpc. This reinforces the conclusion that there is a non-negligible size-environment relation on the red sequence at  $z \sim 0.75$ . The Hodges-Lehmann (H-L) estimator of the mean is given by the median value of the mean computed over all pairs of galaxies in the sample (Hodges & Lehmann 1963). Like taking the median of a distribution, the H-L estimator of the mean is robust to outliers, but, unlike the median, yields results with scatter (in the Gaussian case) comparable to the arithmetic mean. Thus, by using the H-L estimator of the mean, we gain robustness as in the case of the median, but unlike the median, our measurement errors are increased by only a few percent.

In Figure 4, we show the distribution of the differences between the Hodges-Lehmann estimator of the mean size, stellar mass, redshift, Sérsic index, and color for the high-density subsample relative to that for each of the 1000 low-density subsamples, where the median difference in the H-L estimate of the mean size is  $\Delta r_e = 0.559$  (as illustrated by the dashed vertical line) versus  $\Delta \log_{10}(M_*/h^{-2} M_\odot) = -0.002$ ,  $\Delta z = -0.003$ ,  $\Delta n = 0.057$ , and  $\Delta(U - B) = -0.001$  for stellar mass, redshift, Sérsic index, and color, respectively (see Table 2). Within the stellar mass range of

$10 < \log_{10}(M_*/h^{-2} M_\odot) < 11$ , we find significant evidence for a correlation between galaxy size and environment at  $z \sim 0.75$ , such that higher-density regions play host to larger galaxies at a given stellar mass on the red sequence.

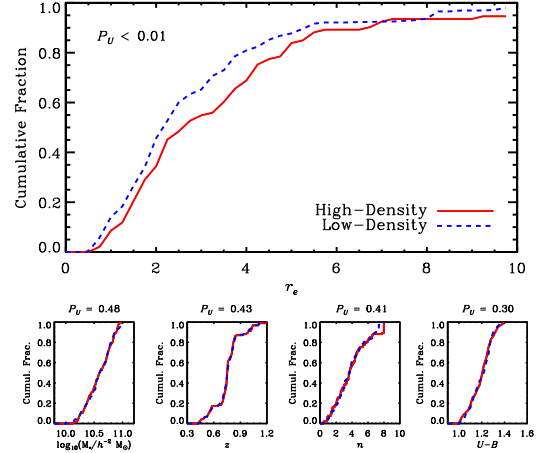


FIG. 3.— the cumulative size ( $r_e$ ), stellar mass, redshift, Sérsic index ( $n$ ), and rest-frame color ( $U - B$ ) distributions for the 93 DEEP2 galaxies comprising the top 15% of the environment distribution within the stellar mass and redshift ranges of  $10 < \log_{10}(M_*/h^{-2} M_\odot) < 11$  and  $0.4 < z < 1.2$  in comparison to the corresponding cumulative distributions for the 1000 random galaxy subsamples drawn from the lowest 50% of the same environment distribution. As discussed in the text, the low-density subsamples, which are each composed of 93 galaxies, are selected to have the same stellar mass, redshift, and Sérsic index distribution as the high-density population. However, the size distribution is found to be significantly different in the different environment regimes.

To test the robustness of our results to the particularities of the sample selection, we repeat the analysis described above for several samples spanning varying redshift and stellar mass regimes. For example, restricting the redshift range over which we select galaxies to  $0.7 < z < 1.2$ , thereby decreasing the size of the sample, we again find a statistically significant relationship between galaxy structure and environment within our adopted stellar mass bin of  $10 < \log_{10}(M_*/h^{-2} M_\odot) < 11$ . For the 64 galaxies in the high-density regime (again the highest 15% of the overdensity distribution) at  $0.7 < z < 1.2$ , the cumulative distribution of galaxy size ( $r_e$ ) is skewed towards larger effective radii relative to the comparison set of galaxies in low-density environments, yielding  $P_U < 0.01$  and a median difference in the H-L estimator of the mean size of  $\Delta r_e \sim 0.63 h^{-1}$  kpc.

An obvious concern when studying the structure of galaxies on the red sequence is the relative contribution of early-type systems and dusty disk galaxies to the sample. Especially at fainter magnitudes/lower stellar mass, reddened star-forming galaxies comprise a significant portion of the red galaxy population (e.g., Lotz et al. 2008; Bundy et al. 2010; Cheng et al. 2011), and as many studies of environment and clustering at intermediate redshift have shown the star-forming population tends to reside in lower-density regions relative to their passive counterparts (e.g., Cooper et al. 2006, 2007; Capak et al. 2007; Coil et al. 2008; Kovač et al. 2010). Even with our primary sample selected to be at the massive end of the red

<sup>21</sup> Note that the two-sided probability for the WMW  $U$  test is given by doubling the one-sided probability. Here, we report only the one-sided probability.

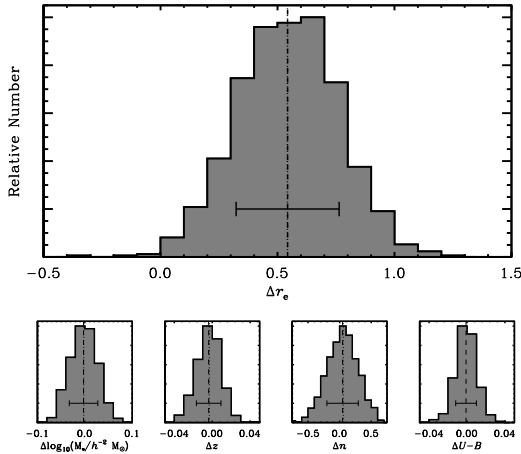


FIG. 4.— the distribution of differences between the Hodges-Lehmann (H-L) estimator of the mean size, stellar mass, redshift, Sérsic index, and rest-frame color for the high-density subsample of 93 red-sequence galaxies at  $0.4 < z < 1.2$  and  $10 < \log_{10}(M_*/h^{-2} M_\odot) < 11$  relative to the corresponding H-L estimator of the mean for each of the 1000 low-density subsamples. The dotted and dashed vertical lines show the median and mean, respectively, of the distribution of differences between the H-L means for each galaxy property; error bars denote the uncertainty in the mean as given in Table 2. We find a significant offset in size of  $\Delta r_e \sim 0.6 h^{-1} \text{ kpc}$  (physical), while the difference in mean stellar mass, redshift, Sérsic index, and color of the two samples is consistent with zero (by construction for all but color).

sequence, disk galaxies ( $n < 2.5$ ) still account for  $\sim 25\%$  of the population (see Figure 3). It is unlikely, however, that a difference in the relative contribution of dusty disk galaxies to the high- and low-density populations is driving the observed size-density relation since galaxy size correlates with Sérsic index such that red disk galaxies (systems with  $n < 2.5$ ) tend to have slightly larger (not smaller) measured sizes than red galaxies of slightly larger Sérsic index. Still, to minimize any potential impact from late-type systems, we define two subsamples: one selected according to  $n > 2.5$  and a second further constrained to systems with  $n > 2.5$  and with axis ratios,  $(b/a)$ , greater than 0.4 (see Table 1). For these subsamples of galaxies with early-type morphology, we find that the correlation between structure and environment persists, reinforcing the conclusion that early-type systems (and not dusty disk galaxies) are responsible for the observed size-density relation at fixed stellar mass.

To illustrate the correlation between size and environment in a more physically intuitive manner, in Figure 5, we show the size-stellar mass relations for early-type galaxies in overdense and underdense regions. In the top portion of Fig. 5, the high- and low-density samples are simply defined to be the extreme quartiles of the environment distribution for all galaxies with  $n > 2.5$ ,  $0.7 < z < 1.2$ , and  $U - B > 1$ . In the middle and bottom panel, however, a more controlled comparison is made, with the high-density sample selected as the top 15% of the environment distribution for all galaxies with  $n > 2.5$ ,  $0.4 < z < 1.2$ , and  $U - B > 1$  and the low-density sample is comprised of  $\sim 400$  galaxies randomly drawn from the bottom 50% of the environment distribution to match the  $z$  distribution (middle) and the joint  $n$  and  $z$  distribution (bottom) of the high-density sample. In agreement with our previous analysis, we find that

within the high-mass segment of the early-type galaxy population the size-stellar mass relation varies with environment, such that galaxies in high-density regions are larger at a given stellar mass.

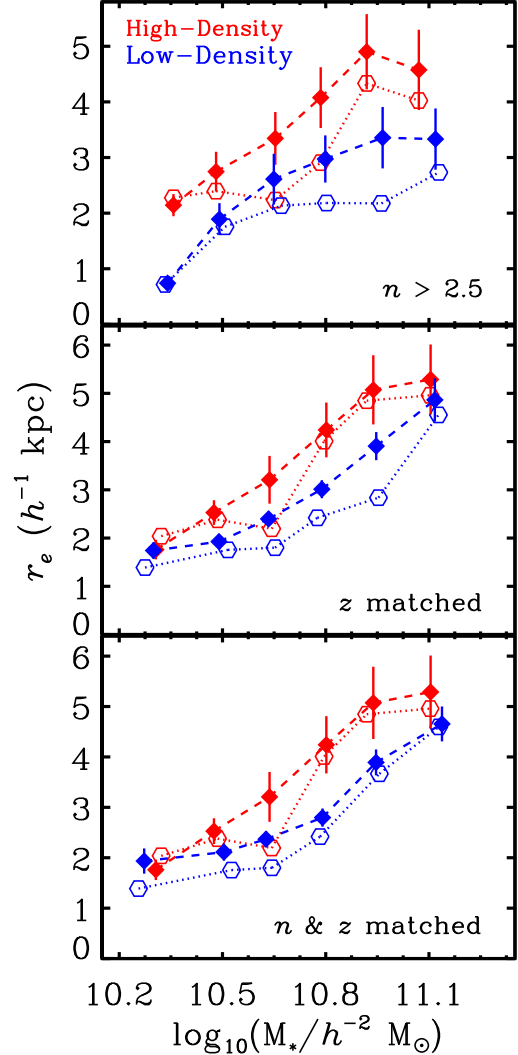


FIG. 5.— the mean (filled diamond connected by dashed lines) and median (open hexagons connected by dotted lines) relationships between galaxy size ( $r_e$ ) and stellar mass in the high-density (red lines and symbols) and low-density (blue lines and symbols) regimes. The means and medians are computed in bins of stellar mass with width  $\Delta \log_{10}(M_*/h^{-2} M_\odot) = 0.3$ . In the *top* panel, the high- and low-density samples are selected as the respective extreme 25% of the environment distribution for all galaxies with  $U - B > 1$ ,  $0.7 < z < 1.2$ , and  $n > 2.5$  — with no matching according to  $n$  or  $z$ . In the *middle* and *bottom* panels, the high-density sample comprises the top 15% of the environment distribution for all galaxies with  $U - B > 1$ ,  $0.4 < z < 1.2$ , and  $n > 2.5$ , with the low-density sample selected from the bottom 50% of the environment distribution so as to have the same  $z$  (and  $n$ ) distributions (but not stellar mass). In both instances, we find that the size-stellar mass relation for early-type galaxies is systematically offset to larger sizes in overdense regions.

Finally, at low surface brightness levels (i.e., low signal-to-noise per pixel in the *HST*/ACS imaging), GALFIT tends to underestimate both galaxy size ( $r_e$ ) and Sérsic index. While such effects are minimal for ob-



jects brighter than the sky background (Häußler et al. 2007), we define a subsample limited to those sources with surface brightness in the *HST*/ACS  $I_{F814W}$  pass-band of  $\mu < 23.5$  magnitudes per arcsec<sup>2</sup> ( $\mu_{\text{sky}} \sim 27.4$ ), which excludes 58 of 623 red galaxies at  $0.4 < z < 1.2$  and  $10 < \log_{10}(M_*/h^{-2} \text{ M}_\odot) < 11$ . For our samples with closely matched stellar mass,  $z$ , and color (i.e., effectively matched apparent magnitude), such a cut on surface brightness imposes an upper limit on physical size, which therefore may impact the observed strength of the size-density relation. However, in spite of this conservative surface brightness limit, we still find a significant relationship between size and local overdensity on the red sequence, with a median difference in the H-L estimator of the mean size of  $\Delta r_e \sim 0.47 h^{-1} \text{ kpc}$ . In Table 1 and Table 2, we list the results from similar analyses of several different galaxy samples. When varying the Sérsic index, stellar mass, surface brightness, axis ratio, and/or redshift regimes probed, we continue to find a significant size-density relation at fixed stellar mass on the red sequence.

#### 4. DISCUSSION

Previous efforts to study the environmental dependence of the size-stellar mass relation at  $z < 2$  within the early-type galaxy population have been relatively few in number and have often found no significant trends with local galaxy density. Comparing the morphologies of massive galaxies in the low-redshift ( $z = 0.165$ ) Abell 901/902 supercluster to those of comparable field samples selected from the Space Telescope A901/2 Galaxy Evolution Survey (STAGES, Gray et al. 2009), Maltby et al. (2010) detect no significant relationship between galaxy structure and environment within the early-type population. Focusing on galaxy groups identified in the Sloan Digital Sky Survey (SDSS, York et al. 2000), a less extreme subdivision of the environment distribution, Guo et al. (2009) also find no significant evidence for a correlation between local environment and the size or Sérsic index within the local early-type population (see also Weinmann et al. 2009; Nair et al. 2010). In contrast, previous studies of brightest cluster galaxies (BCGs) in the local Universe find that BCGs tend to be larger than early-types of comparable stellar mass in less-dense environs (e.g., Bernardi et al. 2007; von der Linden et al. 2007; Desroches et al. 2007; Liu et al. 2008, see also Boylan-Kolchin et al. 2006). However, this environmental dependence apparent in the BCG population is likely the result of cluster-specific mechanisms that drive the formation of this rare subset of the massive early-type galaxy population and may not be indicative of the massive early-type population as a whole. We note that our DEEP2/DEEP3 sample includes very few (if any) systems that will evolve into BCGs at  $z \sim 0$ .

Beyond the local Universe, Valentinuzzi et al. (2010) find no significant variation in the size-stellar mass relation for massive early-types in clusters at  $z \sim 0.7$  relative to that for comparable systems in the field, using data drawn from the ESO Distant Clusters Survey (EDisCS, White et al. 2005). At yet higher redshift, Rettura et al. (2010) compare the sizes of massive ellipticals in an X-ray-luminous cluster at  $z = 1.237$  to those of correspondingly-massive systems in the field, finding

no significant variation in size with environment. Utilizing the same data set, however, Cimatti et al. (2008) propose (though without quantifying) a possible correlation between size and environment similar in nature to that found within our DEEP2/DEEP3 sample (that is, higher-density regions favoring less-compact galaxies). Nevertheless, using largely the same galaxy samples as these two previous studies, recent work from Raichoor et al. (2011) argues for the opposite trend such that galaxies in high-density regions are smaller than their field counterparts. The significance of the measured correlation between size and environment, however, is dramatically overstated by Raichoor et al. (2011), with their results actually consistent with no environment dependence.<sup>22</sup> The lack of a significant environment dependence reported in these previous studies is likely due to [i] the smaller sample sizes employed (the Rettura et al. (2010) and Cimatti et al. (2008) analyses included a total of 45 ellipticals across all environments), [ii] the use of less-precise environment measures (e.g., relying on photometric redshifts such that “field” or low-density samples can be strongly contaminated by group members), and/or [iii] differences in the redshift range probed.

Our results, which show a significant size-density relation at fixed stellar mass within the massive, red galaxy population, suggest that the structural evolution of massive early-type systems occurs preferentially in overdense environments (i.e., groups, given the lack of massive clusters in our sample, Gerke et al. 2005, 2012). This environmental dependence is in general agreement with a model of galaxy formation in which minor, “dry” mergers are a critical mechanism in driving structural evolution at  $z < 2$ . Moreover, our DEEP2/DEEP3 results also suggest that early-types in higher-density regions evolved structurally prior to their counterparts in low-density regions, growing from highly-compact systems at  $z \sim 2\text{--}3$  to more extended systems at  $z \sim 0$ . The earlier onset of this evolution in overdense environments is in agreement with studies of stellar populations locally (e.g., Cooper et al. 2010a) as well as studies of the color-density relation at intermediate redshift (e.g., Cooper et al. 2006, 2007; Gerke et al. 2007), which find that galaxies in high-density environments have typically ceased their star formation earlier than those in less-dense environs. Studies of the Fundamental Plane (FP, Djorgovski & Davis 1987; Dressler et al. 1987) support this picture of accelerated evolution in high-density environments, with several analyses finding that galaxies in high-density regions tend to reach the FP more quickly than those in low-density regions (van Dokkum et al. 2001; Gebhardt et al. 2003; Treu et al. 2005a; Moran et al. 2005).

A correlation between size and environment at fixed stellar mass within the massive early-type population is arguably in conflict with scenarios in which the observed size evolution at intermediate redshift is driven by quasar feedback, as quasars at  $z \sim 1$  are generally not found to reside in overdense environments, especially in relation to the early-type galaxy population. Using cross-correlation techniques and measurements of local envi-

<sup>22</sup> The average sizes for cluster, group, and field early-types as given in Table 1 of Raichoor et al. (2011) are all consistent at the  $1\sigma$  level.

TABLE 1  
SUMMARY OF KS AND WMW  $U$  PROBABILITIES

Sample	$N_{\text{high-density}}$	$\log_{10}(M_*)$ $P_{\text{KS}}$	$P_U$	$z$ $P_{\text{KS}}$	$P_U$	$n$ $P_{\text{KS}}$	$P_U$	$U-B$ $P_{\text{KS}}$	$P_U$	$r_e$ $P_{\text{KS}}$	$P_U$
$0.4 < z < 1.2$ $10 < \log_{10}(M_*) < 11$	93	0.718	0.480	0.605	0.428	0.220	0.413	0.542	0.304	0.011	0.006
$0.7 < z < 1.2$ $10 < \log_{10}(M_*) < 11$	64	0.887	0.421	0.578	0.356	0.562	0.461	0.321	0.280	0.036	0.002
$0.4 < z < 1.05$ $10 < \log_{10}(M_*) < 11$	86	0.807	0.493	0.740	0.445	0.330	0.395	0.614	0.387	0.042	0.020
$0.4 < z < 1.2$ $10.5 < \log_{10}(M_*) < 11$	58	0.795	0.494	0.868	0.452	0.220	0.391	0.379	0.246	0.015	0.013
$0.7 < z < 1.2$ $10 < \log_{10}(M_*) < 11$ $n > 2.5$	42	0.729	0.475	0.725	0.313	0.230	0.384	0.301	0.298	0.007	0.002
$0.7 < z < 1.2$ $10 < \log_{10}(M_*) < 11$ $n > 2.5, b/a > 0.4$	36	0.711	0.476	0.654	0.377	0.252	0.327	0.649	0.393	0.002	0.001
$0.4 < z < 1.2$ $10 < \log_{10}(M_*) < 11$ $\mu < 23.5$	85	0.810	0.499	0.525	0.453	0.594	0.411	0.796	0.364	0.059	0.010

NOTE. — For several galaxy samples, we list the results of the KS and WMW  $U$  tests ( $P_{\text{KS}}$  and  $P_U$ , respectively) from a comparison of the stellar mass, redshift, Sérsic index, color, and size distributions of the respective low- and high-density samples. The  $P$ -values indicate the probability that differences in the distribution of the stated quantity as large as those observed (or larger) would occur by chance if the two samples shared identical distributions. Recall that the  $P_U$  values are one-sided probabilities, while the  $P_{\text{KS}}$  are two-sided. The number of galaxies in the high-density sample (picked to be the top 15% of the environment distribution) is given by  $N_{\text{high-density}}$ . Note that stellar masses and sizes are in units of  $h^{-2} M_\odot$  and  $h^{-1}$  physical kpc, respectively. The samples listed here are matched in stellar mass, redshift, and Sérsic index, by construction.

TABLE 2  
SUMMARY OF DIFFERENCES BETWEEN HODGES-LEHMANN ESTIMATES OF THE MEAN

Sample	$\log_{10}(M_*)$	$z$	$\Delta_{\text{HL}}$ $n$	$U-B$	$r_e$	median of $\Delta_{\text{HL}}$ distribution				
	$\log_{10}(M_*)$	$z$	$n$	$U-B$	$r_e$	$\log_{10}(M_*)$	$z$	$n$	$U-B$	$r_e$
$0.4 < z < 1.2$ $10 < \log_{10}(M_*) < 11$	-0.003 $\pm 0.030$	-0.004 $\pm 0.013$	0.047 $\pm 0.248$	0.001 $\pm 0.011$	0.543 $\pm 0.220$	-0.002	-0.003	0.057	-0.001	0.559
$0.7 < z < 1.2$ $10 < \log_{10}(M_*) < 11$	-0.022 $\pm 0.026$	-0.004 $\pm 0.008$	0.023 $\pm 0.272$	-0.008 $\pm 0.012$	0.688 $\pm 0.251$	-0.005	-0.003	0.075	-0.010	0.632
$0.4 < z < 1.05$ $10 < \log_{10}(M_*) < 11$	0.010 $\pm 0.024$	-0.005 $\pm 0.011$	0.085 $\pm 0.226$	-0.005 $\pm 0.011$	0.393 $\pm 0.209$	-0.003	-0.002	0.078	0.001	0.449
$0.4 < z < 1.2$ $10.5 < \log_{10}(M_*) < 11$	-0.008 $\pm 0.017$	0.001 $\pm 0.015$	0.150 $\pm 0.285$	0.010 $\pm 0.012$	0.619 $\pm 0.274$	-0.003	-0.002	0.085	0.012	0.625
$0.7 < z < 1.2$ $10 < \log_{10}(M_*) < 11$ $n > 2.5$	-0.002 $\pm 0.030$	-0.002 $\pm 0.009$	0.145 $\pm 0.277$	-0.010 $\pm 0.013$	0.802 $\pm 0.239$	-0.002	-0.003	0.090	-0.006	0.826
$0.7 < z < 1.2$ $10 < \log_{10}(M_*) < 11$ $n > 2.5, b/a > 0.4$	-0.003 $\pm 0.030$	-0.005 $\pm 0.016$	-0.128 $\pm 0.301$	-0.006 $\pm 0.013$	0.909 $\pm 0.273$	-0.001	-0.006	0.175	0.000	0.981
$0.7 < z < 1.2$ $10 < \log_{10}(M_*) < 11$ $\mu < 23.5$	0.000 $\pm 0.024$	0.001 $\pm 0.011$	0.083 $\pm 0.214$	-0.001 $\pm 0.010$	0.426 $\pm 0.224$	0.000	0.000	0.050	0.000	0.471

NOTE. — For the same galaxy samples listed in Table 1, we list the mean and median of the distribution of the differences in the Hodges-Lehmann estimator of the mean stellar mass, redshift, Sérsic index, color, and size for the high-density samples relative to that for each of the low-density samples (see Figure 4). Note that stellar masses and sizes are in units of  $h^{-2} M_\odot$  and  $h^{-1}$  physical kpc, respectively. Finally, note that the samples listed here are matched in stellar mass, redshift, and Sérsic index, by construction.

ronment analogous to those presented herein, Coil et al. (2007) find that quasars at  $z \sim 1$  cluster like blue galaxies, such that they favor regions of average galaxy density ( $\log_{10}(1 + \delta_3) \sim 0$ ). While these results suggest that quasars are unlikely to be responsible for the larger sizes of early-types in high-density regions, it should be noted that the clustering measurements of Coil et al. (2007) are roughly  $1-2\sigma$  lower than that of similar studies. For example, Croom et al. (2005, see also Porciani et al. 2004;

Grazian et al. 2004; Myers et al. 2006) find that quasars at  $0.3 < z < 2.2$  have a bias  $\gtrsim 2\sigma$  higher than that found by Coil et al. (2007), while Serber et al. (2006) find an excess of  $\sim L^*$  galaxies on 25 kpc to 1 Mpc ( $h = 0.7$ ) projected comoving scales around quasars at  $z < 0.4$  (see also Hennawi et al. 2006; Myers et al. 2008). For comparison, the median third-nearest-neighbor distance for our sample of early-type galaxies (over all environments) is  $\sim 0.6 h^{-1}$  comoving Mpc in projection. In



addition, Croom et al. (2005) find that the average dark matter halo mass for quasars at intermediate redshift is roughly consistent with (within a factor of a few of) the minimum halos mass inferred for groups at  $z \sim 1$  (Coil et al. 2006, see also Hopkins et al. 2007). Altogether, clustering and environment studies do not support (though also do not clearly exclude) quasars as a viable mechanism for size evolution at  $z < 2$ ; regardless, questions still remain as to how quasar activity would be fueled in a massive early-type system at  $z > 1$ , as the standard scenario involving the major merger of two gas-rich systems (e.g., Springel et al. 2005; Di Matteo et al. 2005; Hopkins et al. 2006) fails to accurately describe massive early-type systems at  $z \gtrsim 1$ , which are relatively gas-poor and have stellar populations with luminosity-weighted ages of  $> 1\text{--}2$  Gyr (e.g., Daddi et al. 2005; Longhetti et al. 2005; Treu et al. 2005b; Schiavon et al. 2006; Combes et al. 2007).

In contrast to quasars, Seyfert galaxies at  $z \sim 1$  typically reside in higher-density environs, similar to those of galaxies on the red sequence (Georgakakis et al. 2007, 2008; Coil et al. 2009; Bradshaw et al. 2011; Digby-North et al. 2011, but see also Silverman et al. 2009). In addition, systems exhibiting line ratios consistent with Low Ionization Nuclear Emission-line Regions (LINERS, Heckman 1980) at  $z \sim 1$ , which tend to reside on the red sequence, are likely to inhabit slightly more overdense regions even relative to galaxies of like color and luminosity (i.e., stellar mass, Yan et al. 2006, 2011; Montero-Dorta et al. 2009; Juneau et al. 2011) — though, recent work suggests that LINERs may not be the product of AGN activity (Yan & Blanton 2011). While lower-luminosity AGN are found in high-density regions at  $z \sim 1$ , consistent with being the driving mechanism behind the observed size evolution of early-type galaxies, the lack of variation in the outflow velocities of winds observed in AGN hosts versus star-forming galaxies suggests that low-luminosity AGN may not play a dominant role in galactic feedback (Rupke et al. 2005; Weiner et al. 2009; Rubin et al. 2010, 2011; Coil et al. 2011, but see also Hainline et al. 2011). Furthermore, the mass loss needed to produce a factor of  $\gtrsim 2$  increase in size is of order 30%–50% (Zhao 2002; Hopkins et al. 2010a), beyond the expected impact of feedback from lower-luminosity AGN or evolved stars (e.g., Damjanov et al. 2009).

## 5. SUMMARY

Using data from the DEEP2 and DEEP3 Galaxy Redshift Surveys, we have completed a detailed study of the relationship between galaxy structure and environment on the massive ( $10 < \log_{10}(M_*/h^{-2} M_\odot) < 11$ ) end of

the red sequence at intermediate redshift. Our principal result is that at fixed stellar mass, redshift, Sérsic index, and rest-frame color we find a significant relationship between galaxy size and local galaxy density at  $z \sim 0.75$ , such that early-type galaxies in high-density regions are more extended than their counterparts in low-density environs. This result is robust to variations in the sample selection procedure, including selection limits based on axis ratio, surface brightness, and Sérsic index. The observed correlation between size and environment is consistent with a scenario in which minor, dry mergers play a critical role in the structural evolution of massive, early-type galaxies at  $z < 2$  and in which the evolution of massive ellipticals is accelerated in high-density regions. Future work, for example from the CANDELS *HST*/WFC3-IR imaging program, will soon enable complementary analyses at yet higher redshift and in more extreme environments such as massive clusters (e.g., Papovich et al. 2011).

MCC acknowledges support for this work provided by NASA through Hubble Fellowship grant #HF-51269.01-A, awarded by the Space Telescope Science Institute, which is operated by the Association of Universities for Research in Astronomy, Inc., for NASA, under contract NAS 5-26555. This work was also supported in part by NSF grants AST-0507428, AST-0507483, AST-0071048, AST-0071198, AST-0808133, and AST-0806732 as well as *Hubble Space Telescope* Archival grant HST-AR-10947.01 and NASA grant HST-GO-10134.13-A. Additional support was provided by NASA through the Spitzer Space Telescope Fellowship Program. MCC acknowledges support from the Southern California Center for Galaxy Evolution, a multi-campus research program funded by the University of California Office of Research. MCC thanks Mike Boylan-Kolchin for helpful discussions in preparing this manuscript and also thanks Greg Wirth and the entire Keck Observatory staff for their help in the acquisition of the DEEP2 and DEEP3 Keck/DEIMOS data. Finally, MCC thanks the anonymous referee for their insightful comments and suggestions that improved this work.

We also wish to recognize and acknowledge the highly significant cultural role and reverence that the summit of Mauna Kea has always had within the indigenous Hawaiian community. It is a privilege to be given the opportunity to conduct observations from this mountain.

*Facilities:* Keck:II (DEIMOS), HST (ACS)

## REFERENCES

- Baldry, I. K., Balogh, M. L., Bower, R. G., Glazebrook, K., Nichol, R. C., Bamford, S. P., & Budavari, T. 2006, *MNRAS*, 373, 469
- Balogh, M. L., Christlein, D., Zabludoff, A. I., & Zaritsky, D. 2001, *ApJ*, 557, 117
- Bell, E. F., McIntosh, D. H., Katz, N., & Weinberg, M. D. 2003, *ApJS*, 149, 289
- Bernardi, M., Hyde, J. B., Sheth, R. K., Miller, C. J., & Nichol, R. C. 2007, *AJ*, 133, 1741
- Bezanson, R., van Dokkum, P. G., Tal, T., Marchesini, D., Kriek, M., Franx, M., & Coppi, P. 2009, *ApJ*, 697, 1290
- Blanton, M. R., Eisenstein, D., Hogg, D. W., Schlegel, D. J., & Brinkmann, J. 2005, *ApJ*, 629, 143
- Bolzonella, M. et al. 2010, *A&A*, 524, A76+
- Bournaud, F., Jog, C. J., & Combes, F. 2007, *A&A*, 476, 1179
- Boylan-Kolchin, M. & Ma, C.-P. 2007, *MNRAS*, 374, 1227
- Boylan-Kolchin, M., Ma, C.-P., & Quataert, E. 2006, *MNRAS*, 369, 1081
- Bradshaw, E. J. et al. 2011, *MNRAS*, 415, 2626
- Bundy, K., Ellis, R. S., & Conselice, C. J. 2005, *ApJ*, 625, 621
- Bundy, K. et al. 2006, *ApJ*, 651, 120
- . 2010, *ApJ*, 719, 1969

- Capak, P., Abraham, R. G., Ellis, R. S., Mobasher, B., Scoville, N., Sheth, K., & Koekemoer, A. 2007, *ApJS*, 172, 284
- Cavaliere, A., Colafrancesco, S., & Menci, N. 1992, *ApJ*, 392, 41
- Cenarro, A. J. & Trujillo, I. 2009, *ApJ*, 696, L43
- Cheng, J. Y., Faber, S. M., Simard, L., Graves, G. J., Lopez, E. D., Yan, R., & Cooper, M. C. 2011, *MNRAS*, 412, 727
- Cimatti, A. et al. 2008, *A&A*, 482, 21
- Coil, A. L., Hennawi, J. F., Newman, J. A., Cooper, M. C., & Davis, M. 2007, *ApJ*, 654, 115
- Coil, A. L., Newman, J. A., Kaiser, N., Davis, M., Ma, C.-P., Kocevski, D. D., & Koo, D. C. 2004, *ApJ*, 617, 765
- Coil, A. L., Weiner, B. J., Holz, D. E., Cooper, M. C., Yan, R., & Aird, J. 2011, *ArXiv e-prints*
- Coil, A. L. et al. 2006, *ApJ*, 638, 668
- . 2008, *ApJ*, 672, 153
- . 2009, *ApJ*, 701, 1484
- Combes, F., Young, L. M., & Bureau, M. 2007, *MNRAS*, 377, 1795
- Conselice, C. J., Bundy, K., U, V., Eisenhardt, P., Lotz, J., & Newman, J. 2008, *MNRAS*, 383, 1366
- Cooper, M. C., Gallazzi, A., Newman, J. A., & Yan, R. 2010a, *MNRAS*, 402, 1942
- Cooper, M. C., Newman, J. A., Madgwick, D. S., Gerke, B. F., Yan, R., & Davis, M. 2005, *ApJ*, 634, 833
- Cooper, M. C. et al. 2006, *MNRAS*, 370, 198
- . 2007, *MNRAS*, 376, 1445
- . 2008, *MNRAS*, 383, 1058
- . 2010b, *MNRAS*, 409, 337
- . 2011, *ApJS*, 193, 14
- Croom, S. M. et al. 2005, *MNRAS*, 356, 415
- Croton, D. J. et al. 2005, *MNRAS*, 356, 1155
- Daddi, E. et al. 2005, *ApJ*, 626, 680
- Damjanov, I. et al. 2009, *ApJ*, 695, 101
- . 2011, *ApJ*, 739, L44+
- Darg, D. W. et al. 2010, *MNRAS*, 401, 1552
- Davis, M. et al. 2003, in *Society of Photo-Optical Instrumentation Engineers (SPIE) Conference Series*, Vol. 4834, Society of Photo-Optical Instrumentation Engineers (SPIE) Conference Series, ed. P. Guhathakurta, 161–172
- Davis, M. et al. 2007, *ApJ*, 660, L1
- Desroches, L.-B., Quataert, E., Ma, C.-P., & West, A. A. 2007, *MNRAS*, 377, 402
- Di Matteo, T., Springel, V., & Hernquist, L. 2005, *Nature*, 433, 604
- Digby-North, J. A. et al. 2011, submitted
- Djorgovski, S. & Davis, M. 1987, *ApJ*, 313, 59
- Dressler, A., Lynden-Bell, D., Burstein, D., Davies, R. L., Faber, S. M., Terlevich, R., & Wegner, G. 1987, *ApJ*, 313, 42
- Efron, B. 1981, *Biometrika*, 68, 589
- Elbaz, D. et al. 2007, *A&A*, 468, 33
- Fakhouri, O. & Ma, C.-P. 2009, *MNRAS*, 394, 1825
- Fan, L., Lapi, A., Bressan, A., Bernardi, M., De Zotti, G., & Danese, L. 2010, *ApJ*, 718, 1460
- Fan, L., Lapi, A., De Zotti, G., & Danese, L. 2008, *ApJ*, 689, L101
- Gebhardt, K., Faber, S. M., Koo, D. C., Im, M., Simard, L., Illingworth, G. D., Phillips, A. C., Sarajedini, V. L., Vogt, N. P., Weiner, B., & Willmer, C. N. A. 2003, *ApJ*, 597, 239
- Georgakakis, A., Gerke, B. F., Nandra, K., Laird, E. S., Coil, A. L., Cooper, M. C., & Newman, J. A. 2008, *MNRAS*, 391, 183
- Georgakakis, A. et al. 2007, *ApJ*, 660, L15
- Gerke, B. F. et al. 2005, *ApJ*, 625, 6
- . 2007, *MNRAS*, 376, 1425
- . 2012, submitted
- Giavalisco, M. et al. 2004, *ApJ*, 600, L93
- Gray, M. E. et al. 2009, *MNRAS*, 393, 1275
- Grazian, A., Negrello, M., Moscardini, L., Cristiani, S., Haehnelt, M. G., Matarrese, S., Omizzolo, A., & Vanzella, E. 2004, *AJ*, 127, 592
- Grogin, N. A. et al. 2011, *ArXiv e-prints*
- Guo, Y. et al. 2009, *MNRAS*, 398, 1129
- Hainline, K. N., Shapley, A. E., Greene, J. E., & Steidel, C. C. 2011, *ApJ*, 733, 31
- Häufler, B., Barden, M., Bamford, S. P., & Rojas, A. 2011, in *Astronomical Society of the Pacific Conference Series*, Vol. 442, Astronomical Society of the Pacific Conference Series, ed. I. N. Evans, A. Accomazzi, D. J. Mink, & A. H. Rots, 155–+
- Häufler, B. et al. 2007, *ApJS*, 172, 615
- Heckman, T. M. 1980, *A&A*, 87, 152
- Hennawi, J. F. et al. 2006, *AJ*, 131, 1
- Hodges, J. R. & Lehmann, E. L. 1963, *The Annals of Mathematical Statistics*, 34, 598
- Hopkins, P. F., Bundy, K., Hernquist, L., Wuyts, S., & Cox, T. J. 2010a, *MNRAS*, 401, 1099
- Hopkins, P. F., Bundy, K., Murray, N., Quataert, E., Lauer, T. R., & Ma, C.-P. 2009a, *MNRAS*, 398, 898
- Hopkins, P. F., Hernquist, L., Cox, T. J., Di Matteo, T., Robertson, B., & Springel, V. 2006, *ApJS*, 163, 1
- Hopkins, P. F., Hernquist, L., Cox, T. J., Keres, D., & Wuyts, S. 2009b, *ApJ*, 691, 1424
- Hopkins, P. F., Lidz, A., Hernquist, L., Coil, A. L., Myers, A. D., Cox, T. J., & Spergel, D. N. 2007, *ApJ*, 662, 110
- Hopkins, P. F., Murray, N., Quataert, E., & Thompson, T. A. 2010b, *MNRAS*, 401, L19
- Juneau, S., Dickinson, M., Alexander, D. M., & Salim, S. 2011, *ApJ*, 736, 104
- Kauffmann, G., White, S. D. M., Heckman, T. M., Ménard, B., Brinchmann, J., Charlot, S., Tremonti, C., & Brinkmann, J. 2004, *MNRAS*, 353, 713
- Khochfar, S. & Silk, J. 2006, *ApJ*, 648, L21
- Kovač, K. et al. 2010, *ApJ*, 718, 86
- Kriek, M. et al. 2006, *ApJ*, 649, L71
- Labbé, I. et al. 2005, *ApJ*, 624, L81
- Lin, L. et al. 2007, *ApJ*, 660, L51
- . 2010, *ApJ*, 718, 1158
- Liu, F. S., Xia, X. Y., Mao, S., Wu, H., & Deng, Z. G. 2008, *MNRAS*, 385, 23
- Longhetti, M. et al. 2005, *MNRAS*, 361, 897
- Lotz, J. M. et al. 2008, *ApJ*, 672, 177
- Maltby, D. T. et al. 2010, *MNRAS*, 402, 282
- Mann, H. B. & Whitney, D. R. 1947, *The Annals of Mathematical Statistics*, 18, 50
- McIntosh, D. H., Guo, Y., Hertzberg, J., Katz, N., Mo, H. J., van den Bosch, F. C., & Yang, X. 2008, *MNRAS*, 388, 1537
- Montero-Dorta, A. D. et al. 2009, *MNRAS*, 392, 125
- Moran, S. M., Ellis, R. S., Treu, T., Smail, I., Dressler, A., Coil, A. L., & Smith, G. P. 2005, *ApJ*, 634, 977
- Myers, A. D., Richards, G. T., Brunner, R. J., Schneider, D. P., Strand, N. E., Hall, P. B., Blomquist, J. A., & York, D. G. 2008, *ApJ*, 678, 635
- Myers, A. D. et al. 2006, *ApJ*, 638, 622
- Naab, T., Johansson, P. H., & Ostriker, J. P. 2009, *ApJ*, 699, L178
- Naab, T., Johansson, P. H., Ostriker, J. P., & Efstathiou, G. 2007, *ApJ*, 658, 710
- Naab, T., Khochfar, S., & Burkert, A. 2006, *ApJ*, 636, L81
- Nair, P. B., van den Bergh, S., & Abraham, R. G. 2010, *ApJ*, 715, 606
- Newman, J. A. et al. 2012, in prep
- Nipoti, C., Treu, T., Auger, M. W., & Bolton, A. S. 2009, *ApJ*, 706, L86
- Oke, J. B. & Gunn, J. E. 1983, *ApJ*, 266, 713
- Papovich, C. et al. 2006, *ApJ*, 640, 92
- . 2011, in prep
- Peng, C. Y., Ho, L. C., Impey, C. D., & Rix, H.-W. 2002, *AJ*, 124, 266
- . 2010, *AJ*, 139, 2097
- Porciani, C., Magliocchetti, M., & Norberg, P. 2004, *MNRAS*, 355, 1010
- Press, W. H., Flannery, B. P., & Teukolsky, S. A. 1986, *Numerical recipes. The art of scientific computing*, ed. Press, W. H., Flannery, B. P., & Teukolsky, S. A.
- Raichoor, A. et al. 2011, *ArXiv e-prints*
- Rettura, A. et al. 2010, *ApJ*, 709, 512
- Rubin, K. H. R., Prochaska, J. X., Ménard, B., Murray, N., Kasen, D., Koo, D. C., & Phillips, A. C. 2011, *ApJ*, 728, 55
- Rubin, K. H. R., Weiner, B. J., Koo, D. C., Martin, C. L., Prochaska, J. X., Coil, A. L., & Newman, J. A. 2010, *ApJ*, 719, 1503
- Rudnick, G. et al. 2009, *ApJ*, 700, 1559
- Rupke, D. S., Veilleux, S., & Sanders, D. B. 2005, *ApJ*, 632, 751
- Schiavon, R. P. et al. 2006, *ApJ*, 651, L93
- Serber, W., Bahcall, N., Ménard, B., & Richards, G. 2006, *ApJ*, 643, 68

- Sérsic, J. L. 1968, *Atlas de galaxies australes*, ed. Sérsic, J. L.
- Silverman, J. D. et al. 2009, *ApJ*, 695, 171
- Springel, V., Di Matteo, T., & Hernquist, L. 2005, *ApJ*, 620, L79
- Taylor, E. N., Franx, M., Glazebrook, K., Brinchmann, J., van der Wel, A., & van Dokkum, P. G. 2010, *ApJ*, 720, 723
- Toft, S., Franx, M., van Dokkum, P., Förster Schreiber, N. M., Labbé, I., Wuyts, S., & Marchesini, D. 2009, *ApJ*, 705, 255
- Treu, T., Ellis, R. S., Liao, T. X., & van Dokkum, P. G. 2005a, *ApJ*, 622, L5
- Treu, T., Ellis, R. S., Liao, T. X., van Dokkum, P. G., Tozzi, P., Coil, A., Newman, J., Cooper, M. C., & Davis, M. 2005b, *ApJ*, 633, 174
- Trujillo, I., Conselice, C. J., Bundy, K., Cooper, M. C., Eisenhardt, P., & Ellis, R. S. 2007, *MNRAS*, 382, 109
- Trujillo, I., Ferreras, I., & de La Rosa, I. G. 2011, *MNRAS*, 415, 3903
- Trujillo, I. et al. 2006, *ApJ*, 650, 18
- Valentinuzzi, T., Poggianti, B. M., Saglia, R. P., Aragón-Salamanca, A., Simard, L., Sánchez-Blázquez, P., D'onofrio, M., Cava, A., Couch, W. J., Fritz, J., Moretti, A., & Vulcani, B. 2010, *ApJ*, 721, L19
- van der Wel, A., Bell, E. F., van den Bosch, F. C., Gallazzi, A., & Rix, H.-W. 2009, *ApJ*, 698, 1232
- van der Wel, A. et al. 2007, *ApJ*, 670, 206
- van Dokkum, P. G., Franx, M., Kelson, D. D., & Illingworth, G. D. 2001, *ApJ*, 553, L39
- van Dokkum, P. G. et al. 2008, *ApJ*, 677, L5
- . 2010, *ApJ*, 709, 1018
- von der Linden, A., Best, P. N., Kauffmann, G., & White, S. D. M. 2007, *MNRAS*, 379, 867
- Wall, J. V. & Jenkins, C. R. 2003, *Practical Statistics for Astronomers* (Princeton Series in Astrophysics)
- Weiner, B. J. et al. 2009, *ApJ*, 692, 187
- Weinmann, S. M., Kauffmann, G., van den Bosch, F. C., Pasquali, A., McIntosh, D. H., Mo, H., Yang, X., & Guo, Y. 2009, *MNRAS*, 394, 1213
- Wetzel, A. R., Schulz, A. E., Holz, D. E., & Warren, M. S. 2008, *ApJ*, 683, 1
- White, S. D. M. et al. 2005, *A&A*, 444, 365
- Williams, R. J., Quadri, R. F., Franx, M., van Dokkum, P., Toft, S., Kriek, M., & Labbé, I. 2010, *ApJ*, 713, 738
- Willmer, C. N. A. et al. 2006, *ApJ*, 647, 853
- Yan, R. & Blanton, M. R. 2011, *ArXiv e-prints*
- Yan, R., Newman, J. A., Faber, S. M., Konidaris, N., Koo, D., & Davis, M. 2006, *ApJ*, 648, 281
- Yan, R. et al. 2011, *ApJ*, 728, 38
- York, D. G. et al. 2000, *AJ*, 120, 1579
- Zhao, H. 2002, *MNRAS*, 336, 159
- Zirm, A. W. et al. 2007, *ApJ*, 656, 66